LANGMUIR

Article

Cite This: *Langmuir* 2019, 35, 13805−13814

pubs.acs.org/Langmuir

Lipid Bilayer Thickness Measured by Quantitative DIC Reveals Phase Transitions and Effects of Substrate Hydrophilicity

David Regan,*,† Joseph Williams,‡ Paola Borri,‡ and Wolfgang Langbein*,†

†School of Physics and Astronomy, Cardiff University, The Parade, Cardiff CF24 3AA, U.K.

‡School of Biosciences, Cardiff University, Museum Avenue, Cardiff CF10 3AX, U.K.

Supporting Information

ABSTRACT: Quantitative differential interference contrast microscopy is demonstrated here as a label-free method, which is able to image and measure the thickness of lipid bilayers with 0.1 nm precision. We investigate the influence of the substrate on the thickness of fluid-phase 1,2-dioleoyl-*sn*-glycero-3-phosphocholine (DOPC)-supported lipid bilayers and find a thinning of up to 10%, depending on substrate hydrophilicity, local bilayer coverage, and ionic strength of the medium. With fluorescently labeled lipid bilayers, we also observe changes in the bilayer thickness depending on the choice of fluorophore. Furthermore, liquid-ordered domains in bilayers, formed from DOPC, cholesterol, and sphingomyelin, are measured, and the corresponding thickness change between the liquid-ordered and liquid-disordered phases is accurately determined. Again, the thickness difference is found to be dependent on the presence of the fluorophore label, highlighting the need for quantitative label-free techniques.

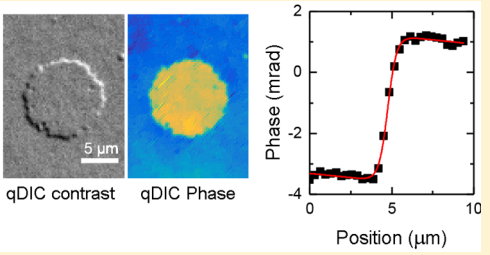

INTRODUCTION

Of all the model systems used to study the properties of biological membranes, supported lipid bilayers (SLBs) are one of the most common.[1,2] Consisting of a stack of one or more lipid bilayers, separated from a solid substrate and each other by hydration layers reported to be 1−2 nm thick,[3] SLBs are favored in part because of the relative ease with which they can be produced.[4] This, coupled with their stability, has allowed them to be used for a wide variety of different studies. These include investigations into membrane mechanical properties,[5] viral entry into cells,[6] micron-scale temperature gradients,[7] and protein−ligand interactions.[8]

One property of SLBs, which differentiate them from typical biological membranes, is their interaction with the substrate. Many experiments on SLBs assume that the effects of the substrate−bilayer interactions on the structure and behavior of the bilayer are negligible. However, while the hydration layer, if present, does prevent direct contact between the bilayer and the support, a multitude of effects of the substrate on bilayer properties has been reported. These include, but are not limited to, decoupling of the phase transition between the two leaflets in the bilayer,[2,9,10] altered interleaflet sorting of lipids,[1,11] a reduced[12] or enhanced[13] capacity to form liquid-ordered (L_o) domains, or altered lipid diffusion rates.[3,12] These effects are known to depend on the substrate material,[1] the chemical modifications applied to the substrate,[5,12] and the ionic strength of the medium.[11]

In spite of all the work carried out thus far, the full extent of the influence of the substrate on the bilayer is not yet known. Notably, the effect of surface hydrophilicity on bilayer thickness has yet to be addressed experimentally. Bilayer thickness is known to modulate protein function,[14] and local bilayer thickness differences have been shown to affect the ability of proteins to interact with domains,[6] so it is important to understand how the support might affect this parameter. While some seek to minimize these assorted substrate effects by increasing the distance between the SLB and the support (through the use of polymer cushions[13] or multilamellar films,[15] for example, which however might introduce other interactions), many experiments are still conducted with the bilayer in close proximity to the support.

A diverse assortment of different techniques has been applied to study SLBs. The use of fluorescent labels is common as a facile way of rendering the SLB visible in optical microscopy, which can also be used to measure lipid diffusion[12,15] and lipid order[16] but is limited by photobleaching. Further, the need to incorporate these labels into the bilayer structure may perturb lipid packing,[17] and the labels themselves have been reported to cause peroxidation of membrane lipids.[13] X-ray and neutron scattering techniques provide high-resolution detail on the internal structure of the lipid bilayer but are technically complex and are ensemble techniques, requiring large volumes of either multilamellar stacks of hundreds of bilayers or dispersions of lipid bilayer vesicles,[18,19] and so are not suited to measure single supported bilayers. Atomic force microscopy (AFM) can generate thickness maps of SLB samples with high axial and lateral

Received: January 14, 2019
Revised: August 13, 2019
Published: September 4, 2019

DOI: 10.1021/acs.langmuir.9b02538
Langmuir 2019, 35, 13805−13814

resolution[9] but cannot distinguish between the thickness of the bilayer itself and the underlying hydration layer.[20]

Quantitative phase imaging is a family of optical microscopy techniques which measure the phase shift of light passing through or reflected from the sample. As the phase shift is proportional to the optical thickness of the sample, quantitative phase techniques require no exogenous contrast agents and can detect extremely small changes in sample thickness and refractive index.[21] Several such techniques have already been applied to model membranes. Variants of digital holographic microscopy have been used to measure lipid bilayer bending elasticity in unilamellar vesicles[22] and image-coexisting lipid phases in multilamellar bilayer stacks,[23] for example, and other forms of quantitative phase microscopy have been used to measure changes in cell membrane potential,[21] tension and bending modulus,[24] and ATP-induced changes in erythrocyte membranes.[25]

Quantitative differential interference contrast (qDIC) is a form of quantitative phase imaging. It generates a quantitative relative phase profile across the sample by effectively integrating images acquired through conventional differential interference contrast using a procedure based on Wiener deconvolution.[26] This qDIC process has previously been used to measure the lamellarity of giant lipid vesicles[26] and has the advantage of being able to produce phase maps using a conventional DIC setup. Here, we show that qDIC is able to determine the optical thickness of individual lipid bilayers with 0.1 nm precision and identify thickness changes resulting from the substrate hydrophilicity and the medium ionicity. Furthermore, as an example of a more biologically relevant application, we use qDIC for the label-free detection of different membrane phases and show the thickness differences between liquid-disordered L_d and liquid-ordered L_o phases.

EXPERIMENTAL SECTION

Lipid mixtures were prepared from stock solutions of 1,2-dioleoyl-*sn*-glycero-3-phosphocholine (DOPC), 1-palmitoyl-2-(dipyrromethene-boron difluoride)undecanoyl-*sn*-glycero-3-phosphocholine (TopFluorPC), chicken egg sphingomyelin (SM), and cholesterol (Chol) in chloroform, which were purchased in powder form from Avanti Polar Lipids (Alabaster, US) and used without further purification. 1,2-Dioleoyl-*sn*-glycero-3-phosphoethanolamine labeled with ATTO488 (ATTO488-DOPE) was purchased in the powder form from ATTO-TEC (Siegen, Germany).

SLBs were prepared by spin coating,[27] using (24 × 24) mm^2 Menzel Gläser (Braunschweig, Germany) glass coverslips as substrates. Coverslips were cleaned by gentle wiping with acetone-soaked cleanroom paper, followed by piranha etching in a mixture of ACS grade sulfuric acid and hydrogen peroxide (30% in H_2O) in a 3:1 volumetric ratio at 95 °C for 1 h. Etched coverslips were stored in nitrogen at 6 °C and used within 2 weeks to retain the surface hydrophilicity, which was quantified before use by depositing 2 μL droplets of distilled water (DW) on the surface and estimating the droplet contact angle (CA) from its radius and volume using the spherical segment assumption described by Chatterjee.[28] While quantitative phase imaging has been applied to directly measure the CA of microdroplets, these change their CA as they rapidly evaporate,[29] which would make it difficult to compare results between different coverslips. Macroscopic water droplets evaporate more gradually but cannot be imaged using our qDIC technique.

An alternative cleaning procedure involved sonicating the glass coverslips for 20 min in baths of toluene, followed by acetone, and then boiling in DW for 3 min. Finally, the coverslip was sonicated in a bath of hydrogen peroxide (30% in H_2O) for at least 20 min. The coverslips were then stored in baths of hydrogen peroxide at the same concentration at 6 °C until needed. This process resulted in a surface hydrophilicity similar to that of piranha-etched coverslips when measured using the previously described hydrophilicity test.

Lipid mixtures were dissolved at 0.8 mg/mL in either 2-propanol or chloroform/acetonitrile (95:5 by volume) for bilayers formed almost exclusively from DOPC. For fluorescence labeling, either DOPE with the fluorophore ATTO488 attached at the head region (H-DOPE) or TopFluorPC (T-PUPC), which has the fluorophore attached to the tail region, was included in the lipid mixture at a concentration of 0.1 mol %. A volume of lipid solution just sufficient for full coverage (typically 300 μL for chloroform/acetonitrile solutions and 150 μL for 2-propanol solutions) was pipetted onto the cleaned glass coverslips mounted in a Laurell WS-650-23 spin coater and then rotated at a speed of 3000 rpm for 30 s, with 6 s acceleration and deceleration stages. All solvents were of HPLC grade purchased from Sigma-Aldrich (St. Louis, US).

After spin-coating, the samples were subjected to a 1 h prehydration process in which the coverslips were placed in a 50 mL centrifuge cylinder containing a small piece of tissue soaked in DW and heated to 37 °C. The cylinder was filled with nitrogen in order to prevent peroxidation of the lipids. The bilayer was then sealed into an enclosed chamber using a microscope slide and a Grace Bio-Labs (Bend, US) SecureSeal imaging spacer. The interior of the chamber was filled with a pH 7.4 phosphate buffered saline (PBS) solution at 1× concentration from Gibco (Gaithersburg, US) or DW, both degassed in vacuum for approximately 5 min immediately before use to eliminate small air bubbles which were visible in DIC. Samples made to investigate liquid−liquid phase coexistence were left for 5 days at 6 °C in order to allow micron-scale L_o domains to form. All others were imaged on the day of preparation.

SLB patches were formed by rupturing giant unilamellar vesicles (GUVs) on piranha-etched glass surfaces. Ten microlitre droplets of 1 mg/mL DOPC/ATTO488-DOPE (99.9:0.1) were deposited on each of two tantalum electrodes, which were placed under vacuum for 1 h to remove the trace solvent. The electrodes were then immersed in DW which had been degassed in vacuum for 5 min, and an ac electric field was applied. For the first hour, the field used square wave modulation at 10 Hz, 1.2 V_{pp}, after which the field was changed to a sinusoidal modulation at 1.5 V_{pp}, at 5 Hz for 30 min, then 2 Hz for 15 min, and then finally 1 Hz for another 15 min. Sixty-five microlitres of this vesicle solution was placed on an etched surface and left for 30 min, at which point 65 μL PBS was added to induce the vesicles to rupture. This was then exchanged with excess PBS to remove free-floating vesicles remaining in the medium.

Fluorescence and DIC images were taken on a Nikon Ti-U inverted microscope using a 20× 0.75 NA dry objective and a 1.5× tube lens, detected by a CCD camera (Hamamatsu Orca 285, having 1344 × 1024 pixels of 6.45 μm size, 18 ke full well capacity, 7 e read noise). A 100 W halogen lamp was used for transillumination. The lamp was switched on 20 min before imaging to ensure that the lamp output was stable. The lamp output was filtered using a Schott BG40 filter (to remove infrared light detected by the camera but outside the operating range of the DIC polarizers) and a Nikon green interference filter to select for a center illumination wavelength λ_0 = 550 nm (50 nm full width at half maximum). Fluorescence illumination used a Prior Lumen 200 lamp with a Semrock GFP-A-Basic-000 filter cube. Nikon ND4 and ND8 filters were used to attenuate the lamp intensity as necessary.

All DIC images were taken using Nikon N2 prisms, providing a shear distance (the separation of the orthogonal polarizations at the sample, providing the shift of the two images forming the differential) measured as (238 ± 10) nm. To reduce image noise, DIC images were averaged over 100 frames, each with 100 ms exposure time, and around 15 ke detected per pixel, resulting in a root-mean-square (rms) shot noise in the single pixel intensity of about 0.08%. The effect of the number of averages on image noise is discussed further in the Supporting Information section S4. To suppress the effects of inhomogeneous illumination, two sets of DIC images $I_{\pm}$ were taken for each region of interest, one with the de-Sénarmont compensator polarizer angle set to either +12.9° or +15° and the other with the polarizer set to the negative of this angle. From each of these image

DOI: 10.1021/acs.langmuir.9b02538
Langmuir 2019, 35, 13805−13814

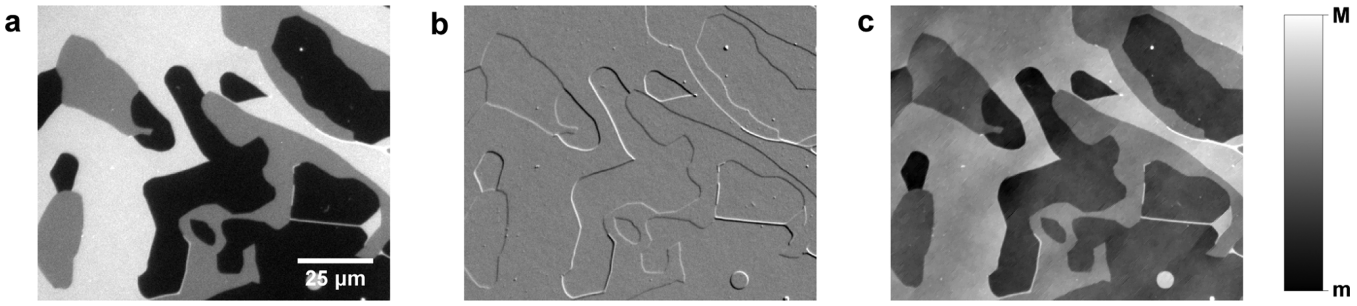

Figure 1. Images of the edge of a DOPC lipid film, showing regions of different lamellarities on a gray scale as given. (a) Fluorescence (M = 600 pe, m = 0 pe), (b) qDIC contrast (m = −0.004, M = 0.004), and (c) qDIC phase (m = −10 mrad, M = 15 mrad). In the fluorescence image, the black regions (~0 pe) correspond to areas where there is no bilayer present, the dark gray regions (~290 pe) are areas where there is a single bilayer on the surface, and the light gray regions are areas of two bilayers (~550 pe). Likewise, in the qDIC phase image, the darker regions correspond to regions of low optical thickness (where there is no bilayer present), while two lighter shades of gray correspond to regions of one or two bilayer thickness.

pairs, a contrast image $I_C = (I_+ - I_-)/(I_+ + I_-)$ was created, which is the measured phase gradient in units of the inverse shear distance. It is then integrated to provide a qDIC phase image, as described in refs.[30,31] Fluorescence images were taken with 1 s exposure time, and intensities are given in detected photoelectrons (pe) per pixel. A weak background (typically around 800 pe/s) measured in regions without lipid was subtracted.

RESULTS AND DISCUSSION

Measuring Bilayers with qDIC. Measurements were made on multilamellar films formed from DOPC labeled with H-DOPE. DOPC is a widely used lipid which forms a single fluid (L_d) phase at room temperature. The different lamellarities in the lipid film are clearly visible in the qDIC images, matching the pattern seen in the corresponding fluorescence images, as shown in Figure 1. Small differences in the position of bilayer edges are due to the time delay between acquisition of the fluorescence and DIC images. Long-range modulations orthogonal to the DIC shear direction are present in the qDIC phase images, which are integration artefacts.[30,31] For clarity, in the figures we present, we show qDIC phase images that have been additionally treated with an energy minimization process (see Supporting Information section S1) to minimize such artefacts unless otherwise stated.

From the integrated qDIC data, the optical thickness of each bilayer can be determined by measuring the phase step over the bilayer edge. All analysis is carried out on the data without energy minimization, as the latter can introduce systematic errors. In order to reduce the influence of the integration artefacts, line profiles were taken roughly along the shear direction (within 13° rms over all profiles), as illustrated in Figure 2. To reduce noise, an average was taken over typically eight pixels perpendicular to the line. The phase step-height was obtained by fitting the function

$$y = \frac{a}{2}\tanh\left(\frac{x-b}{c}\right) + dx + e \quad (1)$$

to the qDIC phase versus position x using nonlinear least squares fitting with the Curve Fitting Tool in MATLAB R2015a. In eq 1, a is the step height, b is the step position, c is the step width, and d and e provide a linear background gradient. An example fit is shown in Figure 2a. In some cases, mostly at double bilayer edges, an additional feature in the phase profile was observed, which was accounted for by the addition of the peak-shaped term $f\,\mathrm{sech}[(x-g)/c]$ to eq 1, where f and g are peak height and position, as shown in Figure 2d. We attribute this feature to the bilayer "rolling over" at the edges of the bilamellar region, resulting in a band of higher phase at the perimeter, an example of which we show in Figure 2f.

The measured phase step height a was then converted into a thickness step height h using

$$h = \frac{a\lambda_0}{2\pi(n_l - n_m)} \quad (2)$$

with the refractive index of the layer, n_l, and of the medium, n_m, and the light wavelength λ_0. Considering that the sample is imaged close to normal incidence, for n_l we use the ordinary refractive index of DOPC, n_{DOPC} = 1.445.[32] For n_m, we use the refractive index of the PBS solution, n_{PBS} = 1.3341,[33] near λ_0 = 550 nm. For the example step shown in Figure 2, the phase step height was found to be (4.49 ± 0.11) mrad. Converting this to absolute thickness and accounting for uncertainties in the refractive index measurements, the width of the wavelength distribution and the confidence limits of the MATLAB fit give a thickness value and associated error on the individual step of (3.78 ± 0.23) nm. To reduce the error, multiple steps were measured over different regions of the bilayer edge and the mean taken.

During imaging, the focusing can vary slightly. We therefore investigated the effect of defocus on the measured thickness, by imaging the same regions at different defocuses. Adjusting the defocus over a range of ±1.2 μm did not significantly alter the mean thickness measured in a given region, as shown in the Supporting Information section S2.

To investigate the influence of the reproducibility of the polarizer settings, the same region of interest was imaged three times, with an independent polarizer calibration each time. When the same steps in each image were measured (see Supporting Information section S3), it was found the mean optical thickness values measured from each image varied by only 0.06 mrad, below the threshold for statistical significance, and corresponding to a thickness variation of 0.05 nm. The precision of the step-height measurement was found to be limited by the roughness of the glass surface, as shown in the Supporting Information section S5.

L_d Phase SLB Thickness. *Effect of the Substrate.* The thicknesses of the different bilayer steps in the lipid film were determined using the discussed procedure. Several different factors affecting the thickness of the SLB were identified. One factor which may influence bilayer thickness is local bilayer

DOI: 10.1021/acs.langmuir.9b02538
Langmuir 2019, 35, 13805−13814

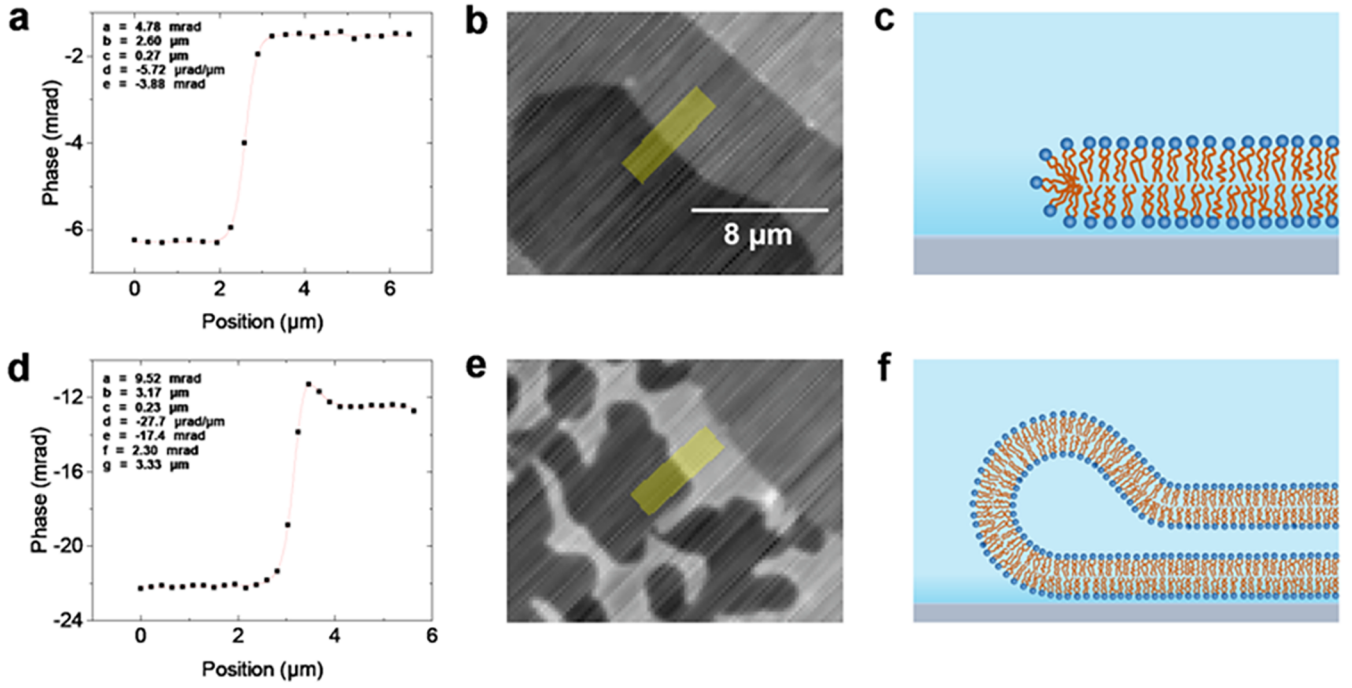

Figure 2. Examples of phase profiles taken over bilayer edges. A typical profile over a single bilayer edge fitted with eq 1 is shown in (a), with (b) showing the corresponding qDIC phase image, on a gray scale (see Figure 1) from −12 to +13 mrad. The region from which the profile was extracted is shaded in yellow. (c) Sketch of a corresponding bilayer edge structure (not to scale). Panel (d) shows a fit to a double bilayer step, incorporating the sech term to accommodate a hump in the phase profile, with (e) showing the corresponding qDIC phase image, on a gray scale from −30 to 0 mrad. (f) Sketch of a corresponding bilayer edge structure. The qDIC phase images (b,e) are not treated with the energy minimization process.

coverage, so to eliminate the influence of coverage, and the data presented in this section are for regions of the sample where the local bilayer coverage is below 90%. The justification for this will be given in the next section.

Using the step from 0 to 1 bilayers, the mean thickness of the first bilayer (the bilayer closest to the support) was found to be 4.08 ± 0.03 nm as a mean of n = 178 steps measured. The second bilayer, measured using the step from 1 to 2 bilayers, showed a thickness of 4.52 ± 0.03 nm (n = 186), which is 0.44 nm larger than the first bilayer. The combined thickness of the first and second bilayers, measured at steps where the edges of the first two bilayers align, was 8.72 ± 0.06 nm (n = 134), consistent with the sum of the individual bilayer thicknesses. All errors given are statistical errors of the mean over n steps. They therefore describe the precision of measurements and do not include systematic errors due to the refractive indices and shear values used in the DIC analysis. The shear value was determined with an error of 4% previously. The refractive index used for the analysis is discussed separately for the different lipid bilayers. A refractive index change by 0.01 leads to a relative thickness change of about 10%. We emphasize that qDIC measures the optical thickness of the layer, and separating this measurement into a thickness and a refractive index requires additional information.

The second bilayer thickness measurements are in good agreement with the thickness of DOPC membranes in DW of 4.57 ± 0.05 nm obtained from X-ray scattering experiments taken at 15 °C,[18] as well as the 4.62 ± 0.15 nm thickness measured in SANS experiments at 25 °C.[19] The observed agreement within 2% indicates that the systematic error due to the refractive index is small.

This observed thickness difference is present in three independent samples prepared using the same preparation conditions (see Section S7) and so is not a random statistical fluctuation. A possible origin of the thickness difference could be that residual sulfur from the piranha-etching process is present on the surface of the coverslip, resulting in peroxidation of the lipids. Such peroxidation would result in reduced bilayer thickness.[34] Indeed, our earlier measurements, which used an older DOPC lipid stock, showed slightly reduced (by ∼0.2 nm) bilayer thicknesses compared with measurements made on bilayers formed from newly ordered DOPC, which we tentatively attribute to slight peroxidation of the lipids. To investigate the possible influence of sulfur, we used the alternative cleaning procedure described in the materials and methods section. This cleaning process gives the glass a hydrophilicity (CA 4.9 ± 0.5°) similar to that produced by piranha-etching, without using sulfur. We find that the relative thickness of the first bilayer compared to the second is 0.897 ± 0.008, in good agreement with the measurements on piranha-etched surfaces and thus contradicting the above hypothesis.

Another possible origin for the thickness difference between the first and second bilayers in the multilamellar film is an interaction between the substrate and the first bilayer, altering the bilayer structure. One surface property already known to affect bilayer behavior is its hydrophilicity, reported for lipid diffusion rates and domain formation within the bilayer,[12] as well as the degree to which bilayers can slide over the support.[5]

To test the hypothesis that interactions with the substrate controlled by hydrophilicity cause the thickness difference, SLBs were formed on glass surfaces with different surface treatments. One substrate was cleaned only by wiping with

DOI: 10.1021/acs.langmuir.9b02538
Langmuir 2019, 35, 13805−13814

acetone-soaked lens paper, and another one was stored in air at room temperature for 4 days after piranha etching. The resulting CAs and bilayer thicknesses are listed in Table 1 and plotted in Figure 3. While the absolute thickness was reduced in the older lipids (see Section S7), the relative changes in bilayer thickness were approximately the same as for the new stock, and so thicknesses are presented relative to the second bilayer thickness of the same sample. For comparison, repeat measurements on a hydrophilic surface taken with new lipid stock are also included. We find that with decreasing surface hydrophilicity, the thickness difference between the first two bilayers decreases, and no statistically significant thickness difference is found for the nonetched surface. Furthermore, no statistically significant difference between the second and third bilayer thickness was observed, independent of surface treatment.

While the surface treatment used changes not only the hydrophilicity measured by the CA but also the surface roughness on an atomistic scale, the hydrophilicity appears to be the relevant quantity, as surfaces treated with hydrogen peroxide, instead of piranha-etching, achieving the same CA, show the same thinning effect.

Computational studies have suggested that a hydrophilic support induces a movement of lipid molecules from the distal (facing away from the support) leaflet to the proximal (support facing) leaflet of the bilayer, driven by the attractive interaction between the lipid headgroups and the support.[4] It is this effect, illustrated in Figure 4, that we hypothesize to be the cause of the changes in the first bilayer thickness. The lipid movement would create two competing effects on the measured bilayer thickness; a loss of lipid density from the distal leaflet which reduces the optical thickness and an increase in lipid density in the lower leaflet which increases the optical thickness. Our data suggest that the former is the dominant effect, consistent with these computational studies. Coarse-grained molecular dynamics simulations[4] have indicated that the resistance of the lower leaflet to compression should result in the bilayer undergoing an overall area expansion with increasing interaction energy, which by volume conservation would lead naturally to the reduction in thickness that we measure experimentally.

In order to explain the observed 10% thickness reduction, the upper leaflet would have to undergo an areal expansion of approximately 20%. This may seem high given that the typical rupture strain of SLBs is around 2%[35] but ruptures require regions of low hydrophobic density in both leaflets in order to form,[36] and the high lipid packing in the lower leaflet would prevent this. The stress in the upper leaflet counterbalances the difference in surface energy between upper and lower leaflets, leading to an equilibrium. The lower leaflet is under a corresponding compressive stress; however, under compression, the leaflet shows a hard-core repulsion,[37] making the strain in the lower leaflet much less than in the upper leaflet, thus not compensating the change in surface density.

As we measure optical thickness which is dependent not only on sample thickness but refractive index as well, the thickness difference, we observe in our data, might be partially caused by a change in refractive index of the bilayer. While we cannot exclude this effect, the 9.7% reduction in thickness we find is in good agreement with computational studies which predict that the thickness of lipid bilayers close to the support would be reduced by 10.6%.[38]

Effect of Labeling. All the measurements described so far have been taken in bilayers including 0.1 mol % head-labeled fluorophore. In order to determine what effect, if any, the choice of fluorophore is having on the bilayer structure, measurements were made of bilayers labeled with 0.1 mol % of a lipid with the fluorophore attached at the tail, T-PUPC, as well as bilayers not containing any fluorescent label.

Interestingly, the thickness difference between the first and second bilayer was lower for the T-PUPC-labeled samples than the H-DOPE-labeled samples, as shown in table Table 2. The

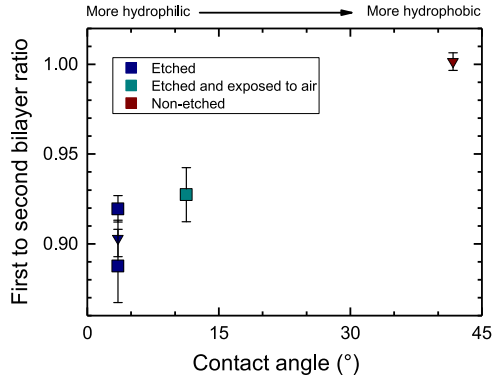

Figure 3. Thickness of the first relative to the second bilayer in supported lipid films formed on substrates with different surface hydrophilicities quantified by the water CA. Squares represent the older lipid stock, while inverted triangles represent data taken with fresh lipid stock.

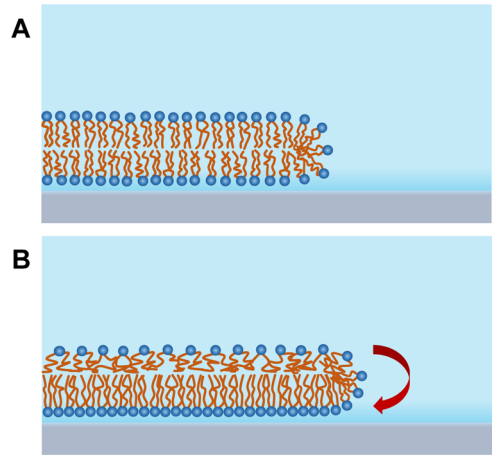

Figure 4. Illustration showing how a trans-leaflet movement of lipids can cause the bilayer thickness to reduce from its initial state (A) to its final equilibrium state (B). The overall bilayer area is increased because of the relative incompressibility of the lower leaflet in response to the movement of lipids.

Table 1. Surface Treatments and Corresponding Bilayer Thicknesses Relative to the Second Bilayer[a]

CA (°)	medium	first bilayer thickness	second bilayer thickness	third bilayer thickness
3.5	PBS	0.919 ± 0.007*	1.000*	0.983 ± 0.025*
11.3	PBS	0.927 ± 0.015*	1.000*	1.011 ± 0.017*
41.7	PBS	1.002 ± 0.005	1.000	0.974 ± 0.014
3.5	DW	0.891 ± 0.028*	1.000*	N/A

[a]Data, which are taken from samples prepared using the older lipid stock, are marked with an asterisk.

DOI: 10.1021/acs.langmuir.9b02538
Langmuir 2019, 35, 13805−13814

Table 2. Measured Thicknesses for Bilayers with Different Fluorophores[a]

fluorophore	first bilayer thickness (nm)	second bilayer thickness (nm)	thickness difference (nm)
H-DOPE	4.08 ± 0.03 (n = 178)	4.52 ± 0.03 (n = 186)	0.44 ± 0.04
T-PUPC	4.13 ± 0.02 (n = 408)	4.37 ± 0.03 (n = 238)	0.24 ± 0.03
none	4.08 ± 0.03 (n = 152)	4.38 ± 0.03 (n = 181)	0.29 ± 0.04

[a]The number of measurements, n, is given in brackets.

thickness of the T-PUPC-labeled samples is effectively the same as for the unlabeled samples, suggesting that the ATTO fluorophore is somehow enhancing the effect of the support on bilayer thickness. It may be that the large ATTO488 fluorophore increases the effective size of the lipid headgroup to an extent which allows it act as an "umbrella", shielding the hydrophobic tails in the upper leaflet from water as the upper leaflet is stretched, in a manner analogous to how cholesterol is shielded from the medium by lipids with larger headgroups. This would reduce the energetic penalty of stretching and shift the equilibrium point toward more lipid movement.

Effect of Coverage. The hypothesis of lipid motion to the lower leaflet requires a lateral edge of the first bilayer, that is, incomplete surface coverage. Without such edges, we would not expect the mechanism to be effective. We have therefore investigated samples of varying surface coverages using data from our early experiments. Lipid films formed from 1.0 mg/mL DOPC/T-PUPC (99.9:0.1) solution with low number of empty regions (average surface coverage 97%) in the first bilayer showed a clear reduction in the thickness difference from the 0.24 nm measured for T-PUPC-labeled bilayers with a large number of empty regions to just 0.09 ± 0.05 nm. When the surface coverage was reduced slightly (to an average of around 80%) by reducing the concentration of the DOPC/T-PUPC mixture to 0.8 mg/mL, the thickness difference between the first and second bilayer increased to 0.18 ± 0.04 nm.

This influence of coverage on the thickness difference is also visible within individual fields of view, as shown in Figure 5. It was found that in fields of view where the relative surface coverage was above 90%, the local difference in thickness between the first and second bilayers reduced, apparently vanishing for near total surface coverage. This is consistent with our hypothesis, as without available free substrate surface, the difference in surface energy does not lead to strain developing in the upper leaflet. In the case of bilayers formed on nonetched surfaces, no relationship between coverage and local thickness difference was observed. Because of this finding, the first bilayer thickness measurements used to explore other effects on the bilayer thickness (such as the previously discussed fluorophore and hydrophilicity effects) were taken only from regions with less than 90% coverage to provide a well-defined regime of the substrate effect. Some images of different bilayer coverages are given in the Supporting Information section S6.

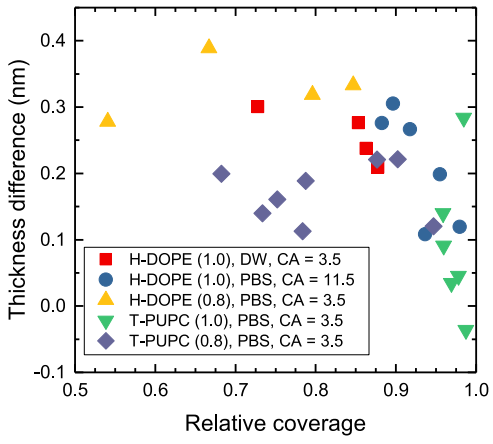

Figure 5. Measured thickness reduction of the first bilayer as function of local surface coverage for PBS or DW hydration media. The concentration of the lipid solution during spin-coating is given in brackets, and the surface hydrophilicity is given by the CA.

Effect of the Medium. Another variable influencing the surface energies is the hydration medium. The PBS solution used has an osmolality between 280 and 315 mOsm/kg (given by the manufacturer) which would screen polar interactions beyond a Debye length of 0.8 nm, thus affecting the interaction between the lipid bilayer and the substrate. Such changes in bilayer−substrate interaction have been shown to alter membrane properties including lipid diffusion and bilayer compression.[15] In order to understand what effects this has on the bilayer thickness, DOPC supported bilayers were prepared using DW as the hydration medium. Bilayers formed in DW tended to have more vesicular structures adhered at bilayer edges, with diameters of a few microns.

The refractive index of the DW hydration medium was taken to be 1.3340,[39] slightly smaller than the PBS refractive index. It was found that the thicknesses of the first and second lipid bilayers were 4.83 ± 0.06 nm (n = 83) and 5.42 ± 0.16 nm (n = 27), respectively, significantly larger than measured for bilayers hydrated in PBS. The thickness difference between the first and second bilayers (measured in regions where the surface coverage was below 0.9) of 0.59 ± 0.17 nm is similar to that observed for bilayers formed in PBS.

Our observation that bilayers are thicker in DW than the relatively high ionic strength PBS solution is surprising given previous literature showing that high ionic strength increases bilayer compression[15,40] and for sufficiently high ionic strengths increases bilayer thickness.[41,42] For example, dual polarization interferometry experiments assuming a fixed, isotropic bilayer refractive index have shown that addition of 2 mM Ca^{2+} increases the thickness of a DOPC bilayer by almost half a nanometre.[43] The nature of the interaction between ions and the lipid bilayer varies greatly depending on the charge, size, valency, and concentration of the ions used,[41] as well as bilayer composition and phase,[42,43] and bilayer thickness has also been found to decrease with increasing osmolarity within certain ionic strength ranges.[42] However, AFM measurements of gel-phase bilayers in PBS solutions with the same ionic strength as used in our experiment have shown an overall increase in lateral bilayer compression,[40] which would be expected to produce an overall increase in bilayer thickness from volume conservation arguments.

Also counter-intuitive is the observation that the change in bilayer thickness is unaffected by the presence or absence of ions, given that multiple experiments have previously demonstrated that the presence of ions can block bilayer−substrate interactions,[15] resulting in the bilayer properties becoming closer to those of a free floating membrane; for bilayers formed on mica, for example, sufficiently high ionic

DOI: 10.1021/acs.langmuir.9b02538
Langmuir 2019, 35, 13805−13814

strengths can prevent decoupling of the main (gel-to-fluid) phase transition on different leaflets of the bilayer.[15]

We can therefore speculate that the bilayer formation pathway has an effect on the measured bilayer thickness. Virtually, all experiments on the effect of ions on the bilayer were conducted using SLBs formed using the vesicle fusion technique, that is, from bilayers which were already formed with both leaflets exposed to the medium. In our preparation procedure instead, a dry lipid film after spin-coating is first hydrated in 100% humidity and then exposed to the hydration medium. This may result in the bilayer−substrate interface forming without a hydration layer or with a reduced hydration layer in the absence of salt ions. The hydration medium might therefore not have sufficient time to penetrate into the substrate—lower leaflet interface.

To investigate this, we formed SLB patches from the rupture of DOPC/H-HOPE (99.9/0.1) GUVs. The open edges of these patches can act as sites of lipid exchange between leaflets similar to the empty areas in the spin-coated bilayers. In this system, the glass substrate is already fully hydrated when the bilayer becomes adhered to the surface. A limitation of the system is that these patches are all unilamellar, so there are no bilamellar regions available for comparison within a single sample. We measure the thickness of this first bilayer to be 4.13 ± 0.05 nm (n = 56). This is in good agreement with the first bilayer measurements made on spin-coated samples on similarly treated surfaces. This suggests that the thickness reduction of the first bilayer is independent of the sample preparation technique.

Summarizing, we find that for fluid-phase DOPC bilayers on hydrophilic substrates, with incomplete surface coverage, the first bilayer has a thickness reduced by about 10% (0.4 nm), which we attribute to the strain in the upper leaflet introduced by the decreased surface energy of the substrate-side leaflet because of the attractive interaction with the substrate.

Liquid-Ordered Domains. Here, we investigate bilayers that show coexistence between liquid-disordered (L_d) and liquid-ordered (L_o) phases, which occurs in ternary mixtures of DOPC, cholesterol (Chol), and SM. The micronscale liquid-ordered domains formed by this lipid mixture are a widely used model for the lipid rafts that appear in biological membranes. Supported bilayers were prepared in PBS from a four component lipid mixture consisting of DOPC/SM/Chol/H-DOPE at a molar ratio of 54.9/25.0/20.0/0.1, which is known to form cholesterol-enriched (L_o) domains at room temperature.[44] While the exact properties of L_o domains vary with composition, they are generally thicker[6,45] and have a higher refractive index[32] than the surrounding liquid-disordered phase, making them visible using qDIC.

Images of a representative region are given in Figure 6. The fluorescence image shows a large homogeneous area, attributed to a single L_d bilayer. This area shows rounded patches with no fluorescence. In qDIC, we find that these patches correspond to convex inclusions in the L_d domain, with optical thicknesses greater than the surrounding L_d bilayer. These are attributed to L_o domains, which are known to exclude H-DOPE.[46] Note that using fluorescence only, the L_o domains cannot be distinguished from holes in the L_d domain, see, for example, the hole in the middle-right of Figure 6. To distinguish them, an additional fluorescent marker of different color enriching in the L_o domains would need to be employed. High-contrast objects in the fluorescence and qDIC images are small vesicles adhered to the surface of the bilayer. More analysis, including

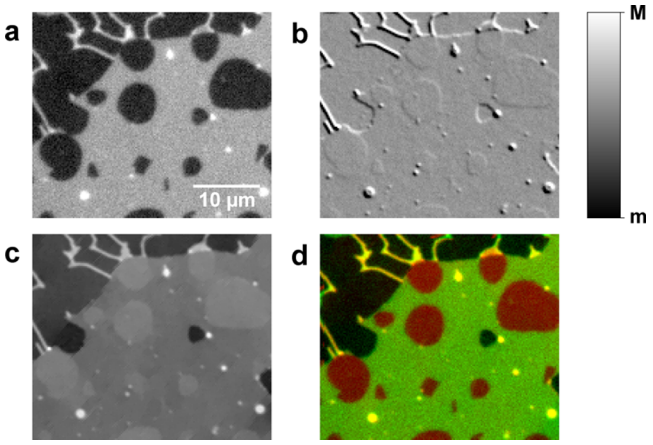

Figure 6. DOPC/SM/Chol/H-DOPE SLB with L_o domains excluding the fluorescent labels, shown in (a) background subtracted fluorescence (m = 0 pe, M = 109 pe), (b) qDIC contrast (m = −0.02, M = +0.02), (c) qDIC phase (m = 1.6 mrad, M = 34.5 mrad), and (d) a composite image showing the phase (red) and fluorescence (green). Imaged at room temperature.

double bilayers, is given in the Supporting Information section S9.

The expected compositional differences between the L_o and the L_d domains are taken into account in the analysis of the height by using slightly different refractive index values of 1.445 for L_d and 1.450 for L_o phases, based on plasmon waveguide resonance measurements of SLBs formed from DOPC and porcine brain SM.[32] The thickness of the L_o phase is then determined by extracting the optical thickness difference over the domain edge by fitting to eq 1, then adding the thickness of the L_d phase which is directly measured at other points on the sample by the same procedure as for the single-component bilayers. The resulting thickness of the L_d phase is (3.90 ± 0.05) nm (n = 48), while that of the L_o phase is (5.19 ± 0.06) nm (n = 48). There was no evidence of significant thickness differences between domains, and also no correlation between thickness and domain size over the 10−800 μm^2 size range that was analyzed (see Supporting Information section S9).

Thin "branch-like" regions are visible, extending from the L_d layer in the top part of the image, which appear to be regions where the bilayer has rolled up on itself to form tubes. The optical thickness and fluorescence of these tubes can be measured by taking line profiles perpendicular to the tube length and integrating the tube line profile. These area measurements are converted to tube circumference values by dividing through the step height of the second bilayer measured in the same modality and the same sample region using eq 1. The results are shown in Figure 7, including results on tubes in a pure L_d-phase DOPC/H-DOPE (99.9/0.1), for comparison. The circumferences obtained from the optical thickness and fluorescence are approximately proportional to each other, with the fluorescence being some 15−20% lower. In a tubular geometry, the birefringence of the lipid bilayer might cause a skew toward higher optical thickness. Using $n_e - n_o$ = 0.01586,[43] there is a 14% increase in optical thickness for the extraordinary index. Assuming a circular geometry, its contribution is half of this for light polarized across the tube and absent for light polarized along the tube. Averaging the two cases leaves a 3.6% increase in optical thickness. Another

DOI: 10.1021/acs.langmuir.9b02538
Langmuir 2019, 35, 13805−13814

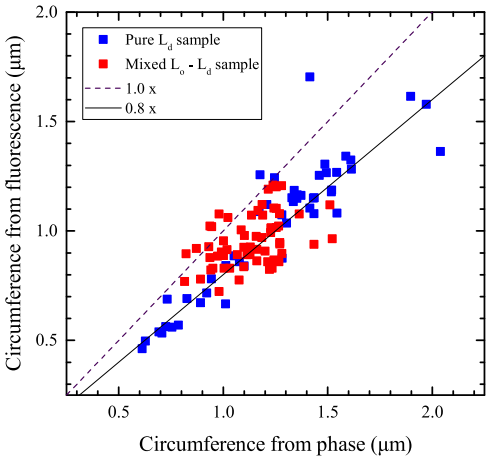

Figure 7. Plot of estimated circumference of tubes from both optical thickness and fluorescence data, for tubes in both a pure L_d phase sample and a sample showing L_o/L_d phase coexistence. The ideal 1:1 relationship between the optical thickness and fluorescence data is shown as a dashed line.

consideration is the orientation of the fluorophore or its steric exclusion from high curvature.

Notably, there is no clear difference in the ratio between the two circumferences between the pure L_d-phase sample and the sample with liquid−liquid phase coexistence, indicating that the tubes are a homogeneous L_d phase. This is expected because L_o domains tend to be excluded from regions of high curvature.[47]

The effect of surface hydrophilicity on the properties of the domains was explored by using an etched coverslip exposed to air as a surface of reduced hydrophilicity. Consistent with our observations on pure DOPC bilayers, the absolute thickness of both phases in the first bilayer of the ternary sample was lower on the more hydrophilic surface, as shown in Figure 8.

The experiment was repeated on a bilayer not containing fluorescent labels, formed from DOPC/SM/Chol (55/25/20). In this sample, the thickness was 3.89 ± 0.03 nm (n = 72) for the L_d phase and 4.96 ± 0.06 nm (n = 84) for the L_o phase. Measuring the phase steps between the coexisting phases, the difference in height between them was found to be 1.06 ± 0.06 nm, significantly smaller than the height difference of 1.29 ± 0.08 nm found in the fluorescently labeled sample. The thickness difference between coexisting domains in the unlabeled bilayers is consistent with the 0.9 ± 0.2 nm value measured for similar lipid compositions[48] using AFM.

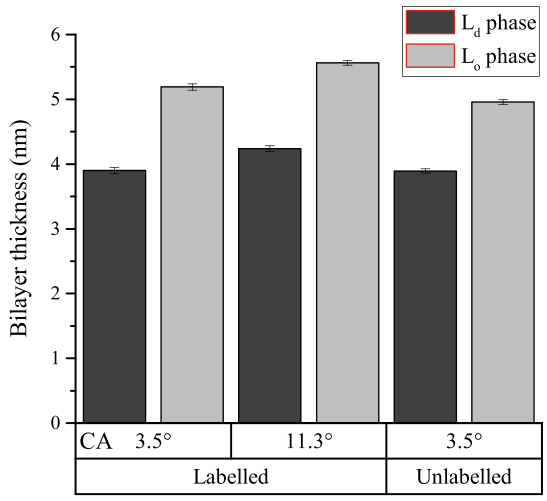

Figure 8. Measured thicknesses of L_o and L_d phases in the first bilayer of DOPC/SM/Chol lipid mixtures under different preparation conditions. Error bars are the standard error of the mean.

The increase in the L_o to L_d thickness difference in the labeled samples by 0.2 nm is surprising, given that such low fluorophore concentrations (0.1 mol %) are generally assumed not to have a significant influence on large-scale bilayer properties.[17] To better understand this finding, we measured the thickness difference in the second bilayer, and find that it is not affected by the fluorophore (see Section S10). The observed effect in the first bilayer can therefore be understood as the result of the H-DOPE fluorophore enhancing the thinning of the L_d phase because of substrate hydrophilicity, as seen in pure L_d-phase bilayers, while the fluorophore-excluding L_o phase is unaffected. The data presented in Table 2 show that the thickness reduction of the L_d phase is 0.2 nm greater in magnitude for bilayers containing 0.1 mol % H-DOPE, consistent with the 0.2 nm difference in the step height between labeled and unlabeled ternary mixtures.

SUMMARY AND OUTLOOK

qDIC imaging has been applied to SLBs in order to provide optical contrast between different bilayer phases not relying on exogenous labels and to precisely measure changes in the thickness of lipid bilayers of known refractive index. The mean thickness values obtained using qDIC on a simple system (DOPC) averaging over more than 100 measurements are in agreement within the 0.1 nm statistical error with measurements taken using X-ray and SANS.

The effect of the substrate on the thickness of lipid bilayers in direct proximity has been measured and found to be dependent on the chemical modifications applied to the surface, with strongly hydrophilic surfaces (CA 3.5°) causing reductions in a first bilayer thickness of up to 0.6 nm, while for untreated glass surfaces (CA 41.7°), the difference was below 0.1 nm. We attribute this behavior to a movement of lipids from the upper to the lower leaflet in order to maximize the number of hydrophilic head groups near the support. The magnitude of this effect is dependent on the choice of fluorophore, with head-labeled lipids enhancing the reduction and tail-labeled lipids not having a noticeable influence on the reduction, as well as the ionic strength of the hydration medium, which is also observed to have an effect on bilayer thickness.

In ternary mixtures of DOPC, cholesterol, and SM, the formation of L_d and L_o domains was imaged, and their thickness is determined to be 3.89 ± 0.03 and 4.96 ± 0.04 nm, respectively. Notably, the thickness difference in the first bilayer was found to be dependent on the presence of the label H-DOPE, with the ordered domains appearing 0.2 nm taller when the label is incorporated into the bilayer, because of the effect of the fluorophore on the L_d phase thickness in the first bilayer.

As an outlook, we emphasize the high sensitivity and image quality obtained with the qDIC method used, which can be performed with widely and commercially available microscopes having DIC contrast and a digital camera. The method allows to observe coexisting phases in lipid bilayers in a label-free and quantitative fashion, enabling the observation of unperturbed systems and separating multiple phases using quantitative

DOI: 10.1021/acs.langmuir.9b02538
Langmuir 2019, 35, 13805−13814

thickness measurements, opening a new paradigm in the study of phase transitions and their dynamics in lipid membranes.

■ ASSOCIATED CONTENT

Supporting Information

The Supporting Information is available free of charge on the ACS Publications website at DOI: 10.1021/acs.langmuir.9b02538.

Energy minimization of the qDIC phase; effect of defocussing on phase measurements; effect of reproducibility of polariser rotation; effect of DIC image averaging on phase measurements; measurement of glass noise; variation of bilayer coverage across sample; absolute thickness values corresponding to table I; domain thickness versus domain area; fluorescence and thickness of double bilayer domains; optical thickness difference between liquid ordered and liquid ordered domains (PDF)

■ AUTHOR INFORMATION

Corresponding Authors

*E-mail: ReganDC@cardiff.ac.uk (D.R.).
*E-mail: langbeinww@cardiff.ac.uk (W.L.).

ORCID

Paola Borri: 0000-0002-7873-3314
Wolfgang Langbein: 0000-0001-9786-1023

Notes

The authors declare no competing financial interest.
The data presented in this work are available from the Cardiff University data archive, http://doi.org/10.17035/d.2019.0067230219.

■ ACKNOWLEDGMENTS

The microscope setup used was developed within the UK BBSRC Research Council (grant n. BB/H006575/1). D.R. and J.W. acknowledge funding by an EPSRC DTA studentship (grant n. EP/M507842/1). P.B. acknowledges the UK EPSRC Research Council for her Leadership fellowship award (grant no. EP/I005072/1). W.L. acknowledges support by his Leverhulme Royal Society Research Fellowship (Grant no. LT20085). The authors thank Iestyn Pope for assistance in the data acquisition, as well as George Zorinyants and Francesco Masia for contributions to the qDIC analysis software.

■ REFERENCES

(1) Richter, R. P.; Maury, N.; Brisson, A. R. On the Effect of the Solid Support on the Interleaflet Distribution of Lipids in Supported Lipid Bilayers. *Langmuir* **2005**, *21*, 299−304.
(2) Feng, Z. V.; Spurlin, T. A.; Gewirth, A. A. Direct Visualization of Asymmetric Behavior in Supported Lipid Bilayers at the Gel-Fluid Phase Transition. *Biophys. J.* **2005**, *88*, 2154−2164.
(3) Tero, R. Substrate Effects on the Formation Process, Structure and Physicochemical Properties of Supported Lipid Bilayers. *Materials* **2012**, *5*, 2658−2680.
(4) Poursoroush, A.; Sperotto, M. M.; Laradji, M. Phase behavior of supported lipid bilayers: A systematic study by coarse-grained molecular dynamics simulations. *J. Chem. Phys.* **2017**, *146*, 154902.
(5) Stubbington, L.; Arroyo, M.; Staykova, M. Sticking and sliding of lipid bilayers on deformable substrates. *Soft Matter* **2017**, *13*, 181−186.
(6) Yang, S.-T.; Kiessling, V.; Tamm, L. K. Line Tension at Lipid Phase Boundaries as Driving Force for HIV Fusion Peptide-Mediated Fusion. *Nat. Commun.* **2016**, *7*, 1−9.
(7) Bendix, P. M.; Reihani, S. N. S.; Oddershede, L. B. Direct Measurements of Heating by Electromagnetically Trapped Gold Nanoparticles on Supported Lipid Bilayers. *ACS Nano* **2010**, *4*, 2256−2262.
(8) Liu, C.; Huang, D.; Yang, T.; Cremer, P. S. Simultaneous Detection of Multiple Proteins that Bind to the Identical Ligand in Supported Lipid Bilayers. *Anal. Chem.* **2015**, *87*, 7163−7170.
(9) Alessandrini, A.; Facci, P. Phase transitions in supported lipid bilayers studied by AFM. *Soft Matter* **2014**, *10*, 7145−7164.
(10) Leonenko, Z. V.; Finot, E.; Ma, H.; Dahms, T. E. S.; Cramb, D. T. Investigation of Temperature-Induced Phase Transitions in DOPC and DPPC Phospholipid Bilayers Using Temperature-Controlled Scanning Force Microscopy. *Biophys. J.* **2004**, *86*, 3783−3793.
(11) Wacklin, H. P. Composition and Asymmetry in Supported Membranes Formed by Vesicle Fusion. *Langmuir* **2011**, *27*, 7698−7707.
(12) Seu, K. J.; Pandey, A. P.; Haque, F.; Proctor, E. A.; Ribbe, A. E.; Hovis, J. S. Effect of Surface Treatment on Diffusion and Domain Formation in Supported Lipid Bilayers. *Biophys. J.* **2007**, *92*, 2445−2450.
(13) Ayuyan, A. G.; Cohen, F. S. Lipid Peroxides Promote Large Rafts: Effects of Excitation of Probes in Fluorescence Microscopy and Electrochemical Reactions during Vesicle Formation. *Biophys. J.* **2006**, *91*, 2172−2183.
(14) Yuan, C.; O'Connell, R. J.; Jacob, R. F.; Mason, R. P.; Treistman, S. N. Regulation of the Gating of BKCaChannel by Lipid Bilayer Thickness. *J. Biol. Chem.* **2007**, *282*, 7276−7286.
(15) Harb, F. F.; Tinland, B. Effect of Ionic Strength on Dynamics of Supported Phosphatidylcholine Lipid Bilayer Revealed by FRAPP and Langmuir-Blodgett Transfer Ratios. *Langmuir* **2013**, *29*, 5540−5546.
(16) Kilin, V.; Glushonkov, O.; Herdly, L.; Klymchenko, A.; Richert, L.; Mely, Y. Fluorescence Lifetime Imaging of Membrane Lipid Order with a Ratiometric Fluorescent Probe. *Biophys. J.* **2015**, *108*, 2521−2531.
(17) Faller, R. Molecular modeling of lipid probes and their influence on the membrane. *Biochim. Biophys. Acta, Biomembr.* **2016**, *1858*, 2353−2361.
(18) Pan, J.; Tristram-Nagle, S.; Kučerka, N.; Nagle, J. F. Temperature Dependence of Structure, Bending Rigidity, and Bilayer Interactions of Dioleoylphosphatidylcholine Bilayers. *Biophys. J.* **2008**, *94*, 117−124.
(19) Gallová, J.; Uhríková, D.; Islamov, A.; Kuklin, A.; Balgavý, P. Effect of cholesterol on the bilayer thickness in unilamellar extruded DLPC and DOPC liposomes: SANS contrast variation study. *Gen. Physiol. Biophys.* **2004**, *23*, 113−128.
(20) Beckmann, M.; Nollert, P.; Kolb, H.-A. Manipulation and Molecular Resolution of a Phosphatidylcholine-Supported Planar Bilayer by Atomic Force Microscopy. *J. Membr. Biol.* **1998**, *161*, 227−233.
(21) Oh, S.; Fang-Yen, C.; Choi, W.; Yaqoob, Z.; Fu, D.; Park, Y.; Dassari, R. R.; Feld, M. S. Label-Free Imaging of Membrane Potential Using Membrane Electromotility. *Biophys. J.* **2012**, *103*, 11−18.
(22) Minetti, C.; Vitkova, V.; Dubois, F.; Bivas, I. New optical method for measuring the bending elasticity of lipid bilayers. *J. Phys.: Conf. Ser.* **2016**, *682*, 012031.
(23) Farzam Rad, V.; Moradi, A.-R.; Darudi, A.; Tayebi, L. Digital holographic microscopy of phase separation in multicomponent lipid membranes. *J. Biomed. Opt.* **2016**, *21*, 126016.
(24) Popescu, G.; Ikeda, T.; Goda, K.; Best-Popescu, C. A.; Laposata, M.; Manley, S.; Dasari, R. R.; Badizadegan, K.; Feld, M. S. Optical Measurement of Cell Membrane Tension. *Phys. Rev. Lett.* **2006**, *97*, 218101.
(25) Park, Y.; Best-Popescu, C. A.; Dasari, R. R.; Popescu, G. Light scattering of human red blood cells during metabolic remodeling of the membrane. *J. Biomed. Opt.* **2011**, *16*, 011013.
(26) McPhee, C. I.; Zoriniants, G.; Langbein, W.; Borri, P. Measuring the Lamellarity of Giant Lipid Vesicles with Differential Interference Contrast Microscopy. *Biophys. J.* **2013**, *105*, 1414−1420.

DOI: 10.1021/acs.langmuir.9b02538
Langmuir 2019, 35, 13805−13814

(27) Mennicke, U.; Salditt, T. Preparation of Solid-Supported Lipid Bilayers by Spin-Coating. *Langmuir* **2002**, *18*, 8172−8177.
(28) Chatterjee, J. Limiting conditions for applying the spherical section assumption in contact angle estimation. *J. Colloid Interface Sci.* **2003**, *259*, 139−147.
(29) Edwards, C.; Arbabi, A.; Bhaduri, B.; Wang, X.; Ganti, R.; Yunker, P. J.; Yodh, A. G.; Popescu, G.; Goddard, L. L. Measuring the Nonuniform Evaporation Dynamics of Sprayed Sessile Microdroplets with Quantitative Phase Imaging. *Langmuir* **2015**, *31*, 11020−11032.
(30) Pope, I.; Payne, L.; Zoriniants, G.; Thomas, E.; Williams, O.; Watson, P.; Langbein, W.; Borri, P. Coherent anti-Stokes Raman scattering microscopy of single nanodiamonds. *Nat. Nanotechnol.* **2014**, *9*, 940.
(31) Williams, J. B. High sensitivity quantitative analysis of differential interference contrast. In preparation.
(32) Devanathan, S.; Salamon, Z.; Lindblom, G.; Grobner, G.; Tollin, G. Effects of sphingomyelin, cholesterol and zinc ions on the binding, insertion and aggregation of the amyloid Abeta1-40 peptide in solid-supported lipid bilayers. *FEBS J.* **2006**, *273*, 1389−1402.
(33) Schoch, R. L.; Kapinos, L. E.; Lim, R. Y. H. Nuclear transport receptor binding avidity triggers a self-healing collapse transition in FG-nucleoporin molecular brushes. *Proc. Natl. Acad. Sci. U.S.A.* **2012**, *109*, 16911−16916.
(34) Jurkiewicz, P.; Olżyńska, A.; Cwiklik, L.; Conte, E.; Jungwirth, P.; Megli, F. M.; Hof, M. Biophysics of lipid bilayers containing oxidatively modified phospholipids: Insights from fluorescence and EPR experiments and from MD simulations. *Biochim. Biophys. Acta, Biomembr.* **2012**, *1818*, 2388−2402.
(35) Staykova, M.; Holmes, D. P.; Read, C.; Stone, H. A. Mechanics of surface area regulation in cells examined with confined lipid membranes. *Proc. Natl. Acad. Sci. U.S.A.* **2011**, *108*, 9084−9088.
(36) Wang, Z.-J.; Frenkel, D. Pore nucleation in mechanically stretched bilayer membranes. *J. Chem. Phys.* **2005**, *123*, 154701.
(37) Ayton, G.; Smondyrev, A. M.; Bardenhagen, S. G.; McMurtry, P.; Voth, G. A. Calculating the Bulk Modulus for a Lipid Bilayer with Nonequilibrium Molecular Dynamics Simulation. *Biophys. J.* **2002**, *82*, 1226−1238.
(38) Hoopes, M. I.; Deserno, M.; Longo, M. L.; Faller, R. Coarse-grained modeling of interactions of lipid bilayers with supports. *J. Chem. Phys.* **2008**, *129*, 175102.
(39) Bashkatov, A. N.; Genina, E. A. Water refractive index in dependence on temperature and wavelength: a simple approximation. *SPIE Proceedings*, 2003; Vol. *5068*.
(40) Fukuma, T.; Higgins, M. J.; Jarvis, S. P. Direct Imaging of Lipid-Ion Network Formation under Physiological Conditions by Frequency Modulation Atomic Force Microscopy. *Phys. Rev. Lett.* **2007**, *98*, 106101.
(41) Pabst, G.; Hodzic, A.; Štrancar, J.; Danner, S.; Rappolt, M.; Laggner, P. Rigidification of Neutral Lipid Bilayers in the Presence of Salts. *Biophys. J.* **2007**, *93*, 2688−2696.
(42) Uhríková, D.; Kučerka, N.; Teixeira, J.; Gordeliy, V.; Balgavý, P. Structural changes in dipalmitoylphosphatidylcholine bilayer promoted by Ca2+ ions: a small-angle neutron scattering study. *Chem. Phys. Lipids* **2008**, *155*, 80−89.
(43) Mashaghi, A.; Swann, M.; Popplewell, J.; Textor, M.; Reimhult, E. Optical Anisotropy of Supported Lipid Structures Probed by Waveguide Spectroscopy and Its Application to Study of Supported Lipid Bilayer Formation Kinetics. *Anal. Chem.* **2008**, *80*, 3666−3676.
(44) Veatch, S. L.; Keller, S. L. Miscibility Phase Diagrams of Giant Vesicles Containing Sphingomyelin. *Phys. Rev. Lett.* **2005**, *94*, 148101.
(45) Bleecker, J. V.; Cox, P. A.; Foster, R. N.; Litz, J. P.; Blosser, M. C.; Castner, D. G.; Keller, S. L. Thickness Mismatch of Coexisting Liquid Phases in Noncanonical Lipid Bilayers. *J. Phys. Chem. B* **2016**, *120*, 2761−2770.
(46) Bartelds, R.; Barnoud, J.; Boersma, A. J.; Marrink, S. J.; Poolman, B. Lipid phase separation in the presence of hydrocarbons in giant unilamellar vesicles. *AIMS Biophys.* **2017**, *4*, 528.
(47) Heinrich, M.; Tian, A.; Esposito, C.; Baumgart, T. Dynamic sorting of lipids and proteins in membrane tubes with a moving phase boundary. *Proc. Natl. Acad. Sci. U.S.A.* **2010**, *107*, 7208−7213.
(48) Rinia, H. A.; Snel, M. M. E.; van der Eerden, J. P. J. M.; de Kruijff, B. Visualizing detergent resistant domains in model membranes with atomic force microscopy. *FEBS Lett.* **2001**, *501*, 92−96.

DOI: 10.1021/acs.langmuir.9b02538
Langmuir 2019, 35, 13805−13814